Supplementary information

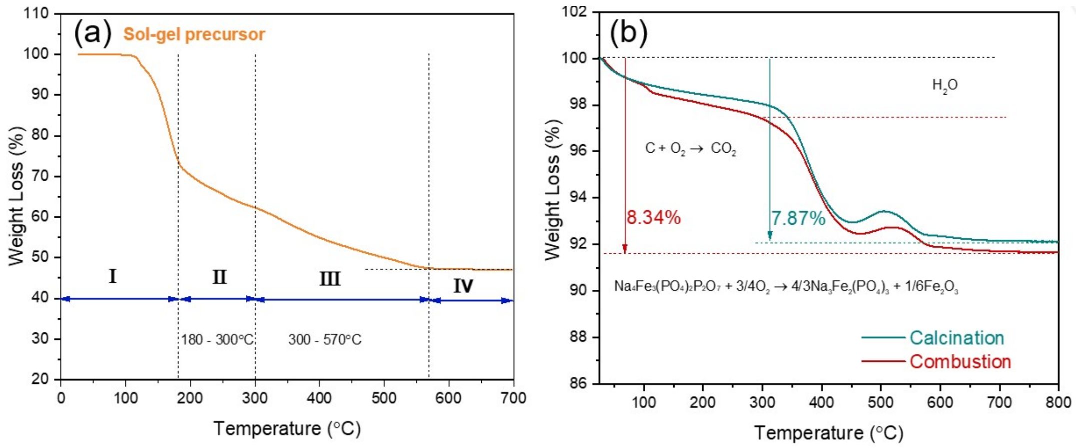

Fig. S1 TG curves of (a) the sol-gel precursor (b) NFPP/CC synthesized by "calcination" and "combustion" methods.

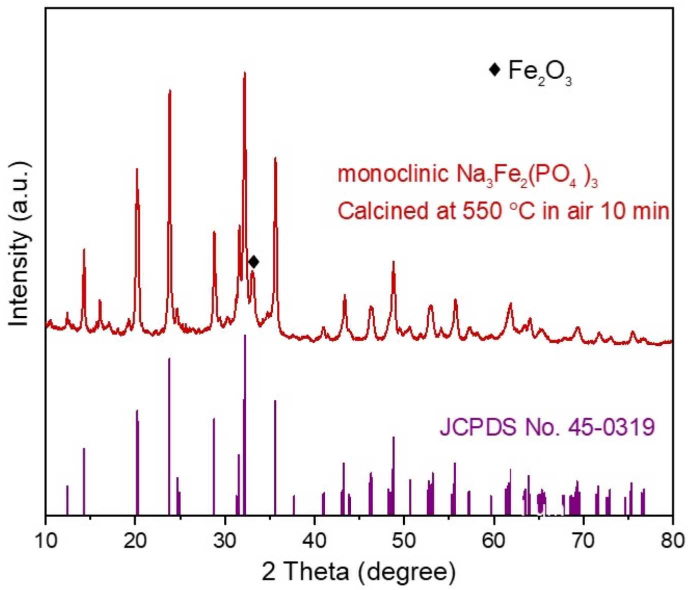

Fig. S2 XRD pattern of sol-gel precursor annealed at 550 °C in air for 10 min.

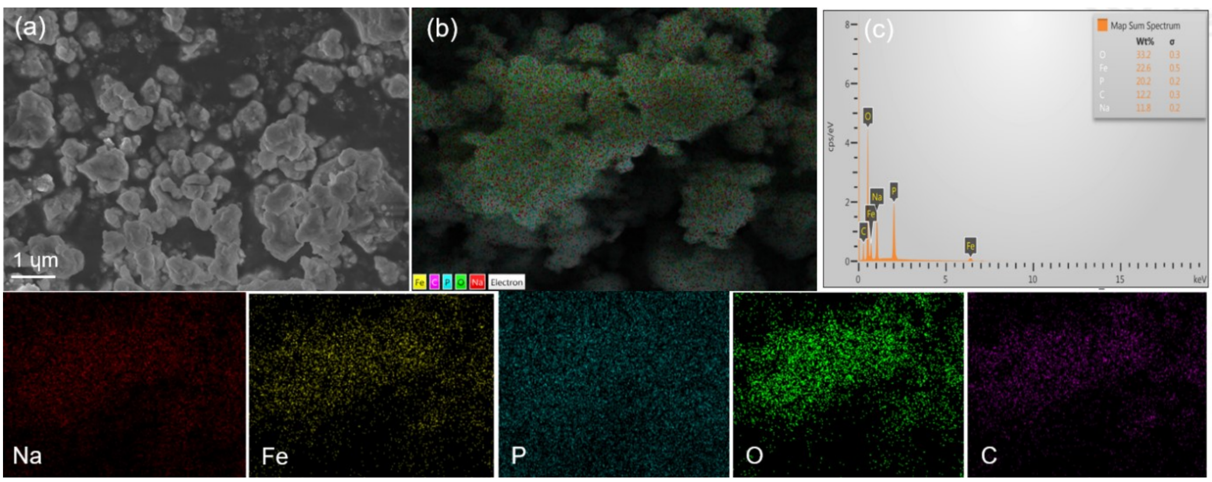

Fig. S3 (a) SEM image of sol-gel precursor annealed at 550 °C in air for 10 min, (b) EDS spectrum and (c) EDS mapping showing the homogeneous distribution of all the elements (Na, Fe, P and O).

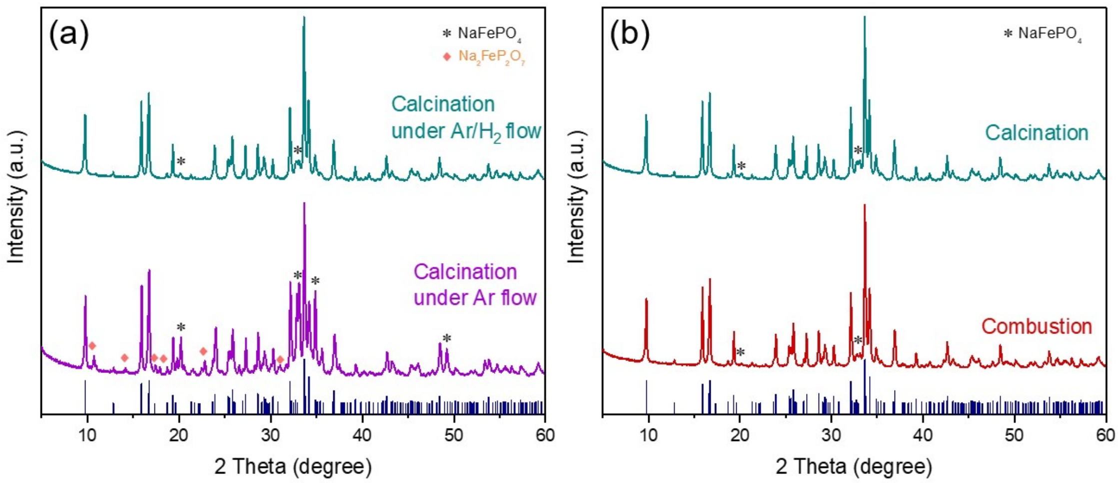

Fig. S4 XRD patterns of NFPP synthesized by (a) "calcination" under Ar and Ar/H_2 (95:5 vol.%) atmosphere, (b) "calcination" and "combustion" both under Ar/H_2 (95:5 vol.%) atmosphere.

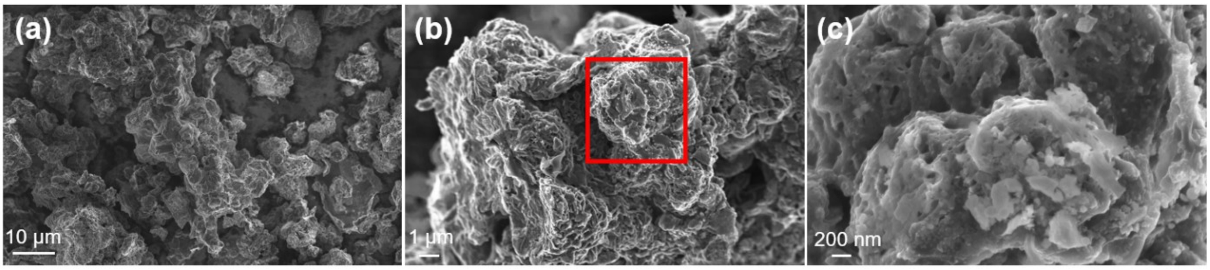

Fig. S5 SEM images of NFPP annealed at 500 °C under inert (Ar) atmosphere showing the impurities as precipitates on the surface.

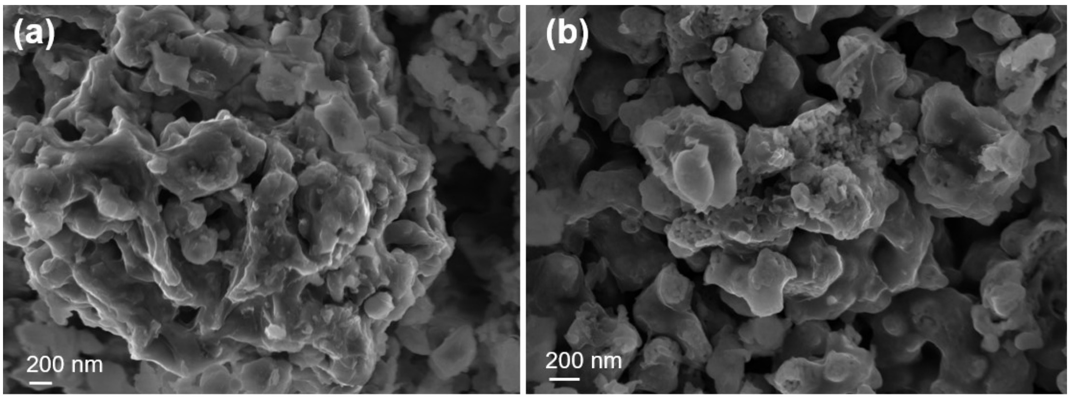

Fig. S6 SEM images of NFPP synthesized by "combustion" method under reducing atmosphere (Ar/H_2 (95:5 vol.%)).

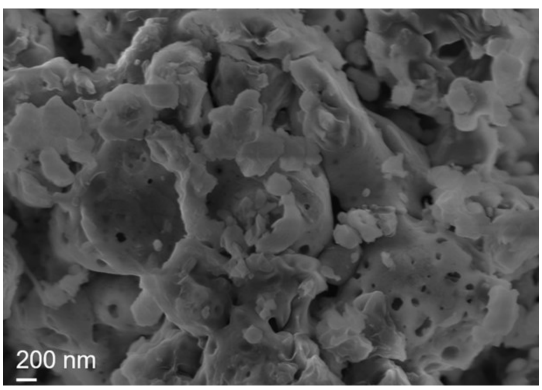

Fig. S7 SEM image of NFPP synthesized by "combustion" method under reducing atmosphere Ar/H_2 (95:5 vol.%) showing nanoporous structure.

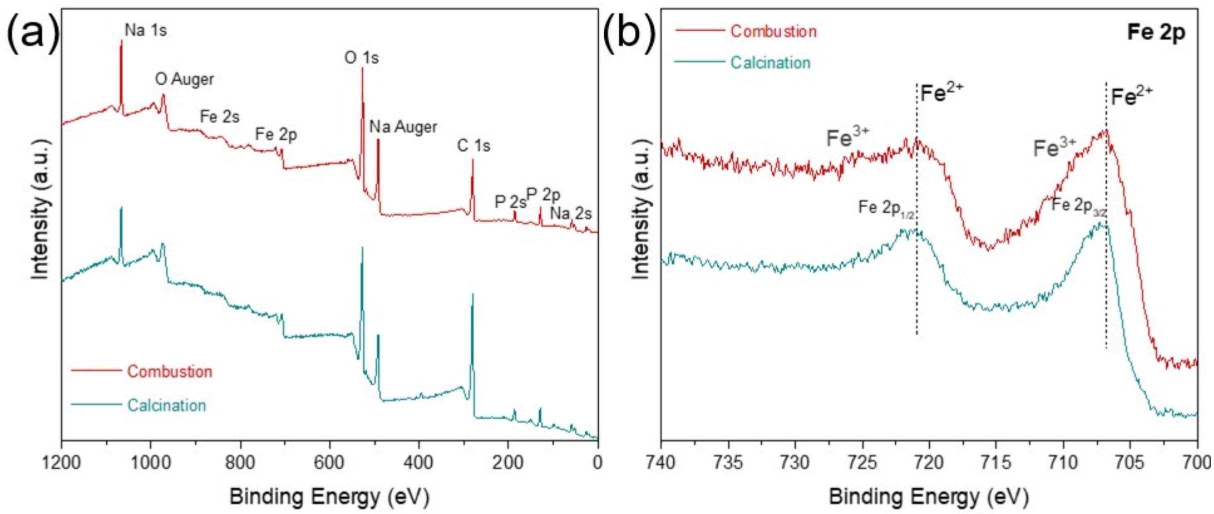

Fig. S8 (a) XPS survey spectra, and (b) Fe 2p spectra of NFPP synthesized by "calcination" and "combustion".

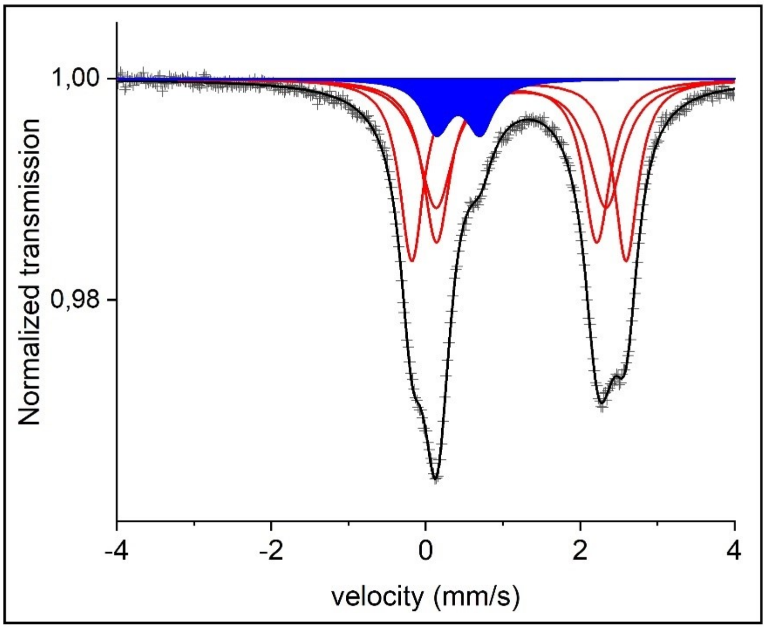

Fig. S9 Room temperature 57Fe Mössbauer spectra of Calcination synthesized pristine $Na_4Fe_3(PO_4)_2(P_2O_7)$. The red and blue marked resonance lines represent high spin Fe^{2+} and Fe^{3+} valences.

The cyclic voltammetry (CV) measurements were performed to investigate the Na^+ insertion/extraction behavior in the NFPP cathodes, providing valuable insights into the electrochemical reactivity and kinetic properties of the materials synthesized under different calcination atmospheres. The CV profiles of NFPP produced by "calcination" method in half-cells presented in **Fig. S10b** reveal several redox peaks correspond to the insertion/extraction of Na^+ ions from different sites namely Na1, Na2, Na3, and Na4 within the NFPP structure [1, 2]. Two main redox couples are observed at 2.95/2.89 and 3.24/3.20 V, accompanied multiple weak redox peaks, representing multi-step Na^+ extraction process from the NFPP structure. The oxidation peaks below 3.0 V are attributed to the transformation of $Na_4Fe_3(PO_4)_2(P_2O_7)$ to $Na_2Fe_3(PO_4)_2(P_2O_7)$, involving the Na^+ extraction from Na3 (5-coordinated) and the Na1 (6-coordinated) sites. Notably, Na2 does not participate in the charging and discharging process and the oxidation state of Fe around Na2 remains unchanged [3, 4]. The oxidation peaks above 3.0 V correspond to the phase transformation of $Na_2Fe_3(PO_4)_2(P_2O_7)$ to $Na_1Fe_3(PO_4)_2(P_2O_7)$

associated with the Na^+ extraction from Na4 (6-coordinated) site [5, 6]. After 1st charge, a peak at 2.80 V emerges because of a minor structural rearrangement (**Fig. S10b**). From the 2nd to 5th cycle, the overlapping of reduction peaks and the small voltage gap demonstrate the high reversibility of Na^+ deintercalation within the NFPP structure [7]. For the sample calcined under an inert atmosphere (Ar) (**Fig. S10a**), a small peak around 2.51 V is observed, indicating the presence of $Na_2FeP_2O_7$ impurity [8, 9]. In contrast, the higher purity NFPP calcined under reducing atmosphere (**Fig. S9b**) does not exhibit any peak related to the impurity which is consistent with the XRD result. The differential capacity curves (dQ/dV) (**Fig. 5b**) of the "combustion" synthesized one also shows the same redox peaks and good reversibility which is consistent with the CV curves.

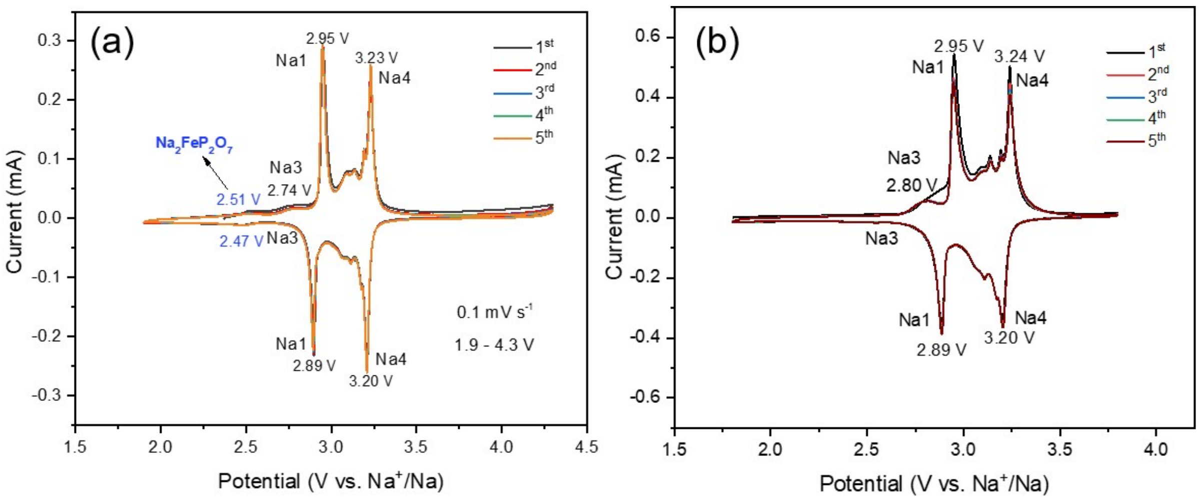

Fig. S10 CV curves for the first five cycles at a scan rate of 0.1 mV s^{-1} at the voltage range of 1.9–4.3 V (vs. Na^+/Na) of "calcination" samples calcinated under (a) inert atmosphere, (b) reducing atmosphere.

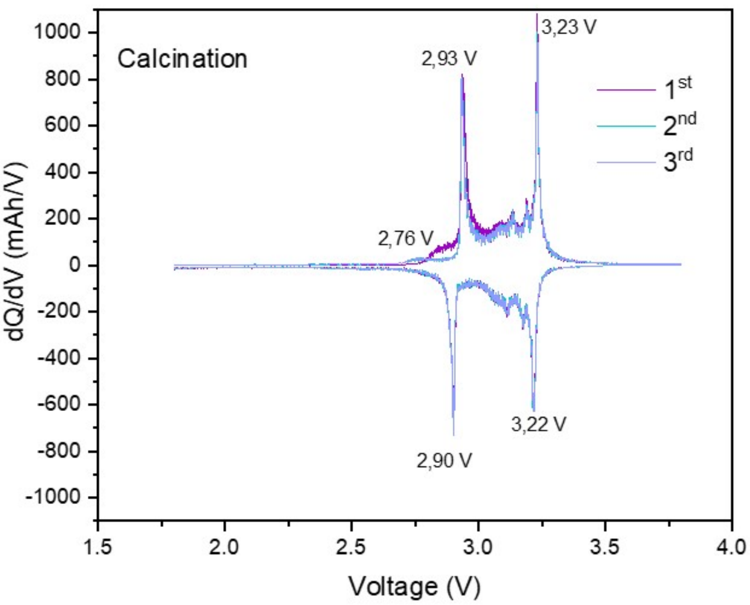

Fig. S11 Differential capacity vs. voltage (dQ/dV) plots for 3 cycles of "calcination" sample.

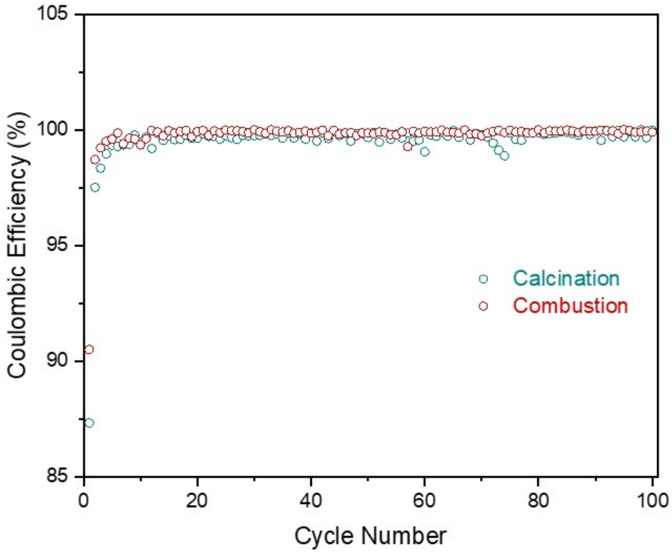

Fig. S12 Coulombic efficiency values of NFPP synthesized by “calcination” and “combustion” for 100 cycles.

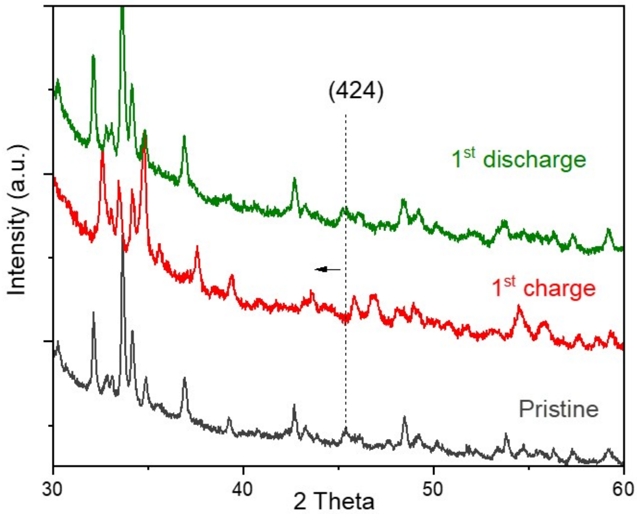

Fig. S13 Ex-situ XRD patterns of NFPP “combustion” pristine electrode, after first charge and after first discharge.

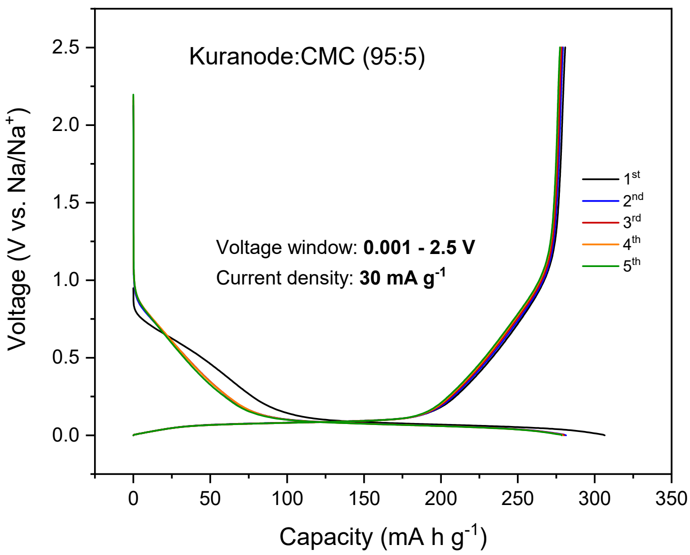

Fig. S14 Charge-discharge curves of hard carbon used in this study at a current density of 30 mA g^{-1}.

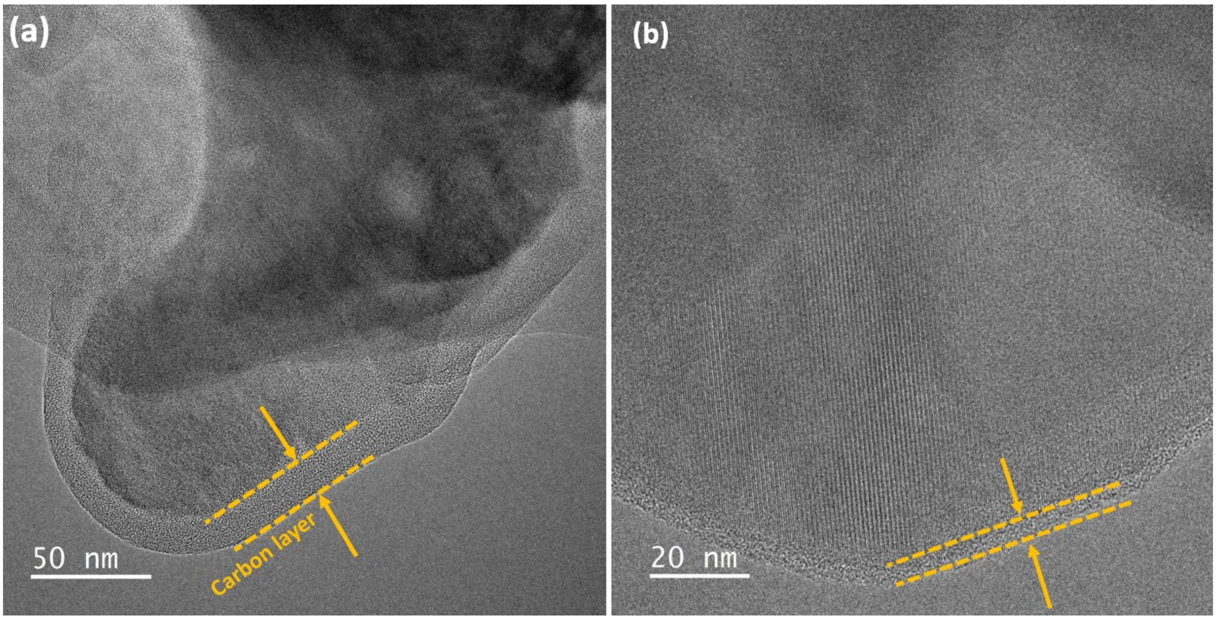

Fig. S15 HRTEM images of (a) "calcination" and (b) "combustion" samples showing the in-situ carbon layer.

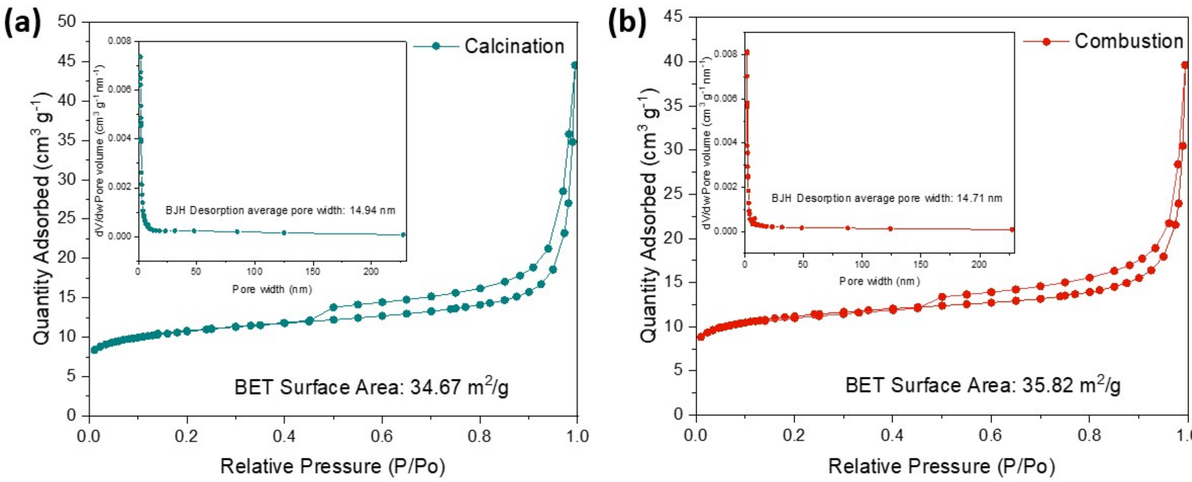

Fig. S16 Nitrogen adsorption–desorption isotherm and pore-size distribution of (a) "calcination" and (b) "combustion" samples.

Table S1. Detailed results of the Rietveld refinement of the "combustion" sample for the NFPP phase. Refinement quality factors are also included. For simplicity, the atomic displacement parameter was fixed to 0.5 Å^2 for all atoms. The occupancy of the Na positions was refined, but for all position except Na2 the value refined to slightly above 1.0. Hence these values were fixed and only Na2 refined.

Lattice parameters (Å)				
a	**b**	**c**	**R_{wp}**	**χ^2**
18.0945(4)	6.5384(2)	10.6536(3)	6.04%	2.12

Site	**x**	**y**	**z**	**Occ**	**B_{iso} (Å^2)**
Fe1	0.3372(2)	0.1241(19)	0.4974(9)	1	0.5
Fe2	0.1310(3)	0.6301(16)	0.4911(8)	1	0.5

Fe3	0.2413(4)	0.3521(11)	0.7471(9)	1	0.5
P1	0.2984(6)	0.6273(37)	0.4969(17)	1	0.5
P2	0.1780(5)	0.1131(31)	0.4885(17)	1	0.5
P3	0.5631(5)	0.4783(17)	0.7386(16)	1	0.5
P4	0.4464(6)	0.1716(17)	0.7313(11)	1	0.5
Na1	0.4954(9)	0.8329(27)	0.9823(14)	1	0.5
Na2	0.2960(6)	0.8781(22)	0.7431(19)	0.95(1)	0.5
Na3	0.3986(7)	0.4597(22)	0.2577(22)	1	0.5
Na4	0.4656(7)	0.7017(20)	0.5416(12)	1	0.5
O1	0.2393(13)	0.5795(54)	0.5982(32)	1	0.5
O2	0.3464(18)	0.4459(51)	0.4607(22)	1	0.5
O3	0.3481(16)	0.8010(52)	0.5304(23)	1	0.5
O4	0.2403(13)	0.6291(66)	0.3903(30)	1	0.5
O5	0.2371(12)	0.1186(55)	0.6149(27)	1	0.5
O6	0.1216(14)	-0.0754(41)	0.5020(22)	1	0.5
O7	0.2279(13)	0.0899(49)	0.3829(28)	1	0.5
O8	0.1358(13)	0.2984(45)	0.4711(25)	1	0.5
O9	0.4871(13)	0.4148(40)	0.6848(21)	1	0.5
O10	0.5400(13)	0.5968(44)	0.8684(23)	1	0.5
O11	0.6225(9)	0.3160(31)	0.7498(34)	1	0.5
O12	0.5809(9)	0.6435(55)	0.6364(18)	1	0.5
O13	0.4468(13)	0.1105(43)	0.8640(27)	1	0.5
O14	0.3711(9)	0.1992(29)	0.6907(21)	1	0.5
O15	0.4873(12)	0.0273(31)	0.6519(22)	1	0.5

Table S2. Detailed results of the Rietveld refinement of the "calcination" sample for the NFPP phase. Refinement quality factors are also included. For simplicity, the atomic displacement parameter was fixed to 0.5 Å^2 for all atoms. The occupancy of the Na position was refined, but for all position except Na2 the value refined to slightly above 1.0. Hence the values were fixed and only Na2 refined.

Lattice parameters (Å)					
a	**b**	**c**		**R_{wp}**	**χ^2**
18.1039(4)	6.5392(2)	10.6545(3)		5.77 %	1.68
Site	**x**	**y**	**z**	**Occ**	**B_{iso} (Å^2)**
Fe1	0.3374(2)	0.1236(19)	0.4982(9)	1	0.5
Fe2	0.1399(3)	0.6320(15)	0.4914(8)	1	0.5
Fe3	0.2416(4)	0.3511(11)	0.7474(10)	1	0.5
P1	0.2987(6)	0.6287(35)	0.4990(17)	1	0.5

P2	0.1781(5)	0.1103(27)	0.4864(18)	1	0.5
P3	0.5637(5)	0.4762(17)	0.7377(17)	1	0.5
P4	0.4479(6)	0.1698(17)	0.7307(11)	1	0.5
Na1	0.4942(10)	0.8342(28)	0.9795(13)	1	0.5
Na2	0.2962(6)	0.8763(22)	0.7449(19)	0.96(1)	0.5
Na3	0.3990(7)	0.4597(22)	0.2590(22)	1	0.5
Na4	0.4642(7)	0.6965(20)	0.5421(11)	1	0.5
O1	0.2385(13)	0.5845(63)	0.6009(34)	1	0.5
O2	0.3471(19)	0.4475(51)	0.4649(23)	1	0.5
O3	0.3455(17)	0.8063(54)	0.5342(23)	1	0.5
O4	0.2438(13)	0.6353(67)	0.3909(31)	1	0.5
O5	0.2354(13)	0.1205(55)	0.6167(27)	1	0.5
O6	0.1192(14)	-0.0709(41)	0.5038(23)	1	0.5
O7	0.2283(14)	0.0876(54)	0.3877(30)	1	0.5
O8	0.1353(14)	0.3055(44)	0.4721(25)	1	0.5
O9	0.4869(14)	0.4158(42)	0.6821(21)	1	0.5
O10	0.5408(13)	0.5942(42)	0.8664(25)	1	0.5
O11	0.6217(9)	0.3187(32)	0.7511(33)	1	0.5
O12	0.5832(10)	0.6433(56)	0.6421(19)	1	0.5
O13	0.4463(13)	0.1129(42)	0.8636(28)	1	0.5
O14	0.3709(10)	0.2027(29)	0.6934(21)	1	0.5
O15	0.4881(13)	0.0299(31)	0.6487(22)	1	0.5

Table S3. Results of the fitting procedure of the 295 K Mössbauer spectra. CS is the center shift relative natural α-Fe held at 295K, |QS| is the magnitude of the electric quadrupole splitting, W is the FWHM Lorentzian line. Error in these parameters are ± 0.05 mm/s. A stands for the spectral area and its error is ± 2%. HS stands for high spin. %. Errors are in parenthesis in the main text.

a) "Combustion" $Na_4Fe_3(PO_4)_2(P_2O_7)$

Pattern	CS (mm/s)	|QS| (mm/s)	W (mm/s)	A %	Fe valence
FeX	1.22	2.75	0.39	31	HS Fe^{2+}
FeY	1.26	2.11	0.47	31	HS Fe^{2+}
FeZ	1.16	2.08	0.42	31	HS Fe^{2+}
FeW	0.44	0.57	0.40	7	HS Fe^{3+}

b) De-sodiated "Combustion" $NaFe_3(PO_4)_2(P_2O_7)$

Pattern	CS (mm/s)	|QS| (mm/s)	W (mm/s)	A %	Fe valence
FeA	0.42	0.38	0.30	30	HS Fe^{3+}

FeB	0.43	0.53	0.40	30	HS Fe^{3+}
FeC	0.43	1.03	0.39	30	HS Fe^{3+}
FeD	1.16	2.42	0.62	10	HS Fe^{2+}

c) "Calcination" $Na_4Fe_3(PO_4)_2(P_2O_7)$

Pattern	CS (mm/s)	|QS| (mm/s)	W (mm/s)	A %	Fe valence
FeX	1.21	2.78	0.37	30	HS Fe^{2+}
FeY	1.24	2.20	0.53	30	HS Fe^{2+}
FeZ	1.18	2.08	0.42	30	HS Fe^{2+}
FeW	0.42	0.60	0.42	10	HS Fe^{3+}

Table S4. Overview of electrochemical performances of NFPP cathode reported with various synthesis approaches.

Electrode material	Synthesis method	Carbon content (%)	Mass loading ($mg\ cm^{2-}$)	Specific capacity	Capacity retention after cycles	Ref.
NFPP calcination	sol-gel	10.55	4-5	88 mAh g^{-1} at 0.1 C	98.7% (100th at 0.1C)	This work
NFPP combustion	modified combustion	5.09		102 mAh g^{-1} at 0.1 C	99.7% (100th at 0.1C)	
NFPP@rGO	spray drying	8.3	1.5	128 mAh g^{-1} at 0.1 C 101 mAh g^{-1} at 10 C 60 mAh g^{-1} at 100 C	62.3% (6000th at 10 C) 88% (1300th at 1 C)	[10]
$Na_4Fe_3(PO_4)_2(P_2O_7)$	sol-gel	8.3	-	110 mAh g^{-1} at 0.05 C 78 mAh g^{-1} at 10 C	89% (300th at 0.5 C)	[1]
$Na_4Fe_3(PO_4)_2(P_2O_7)/C$ @MWCNTs	spray drying	-	7	115 mAh g^{-1} at 0.1 C 62 mAh g^{-1} at 20C	95% (1200th at 2 C)	[11]
$Na_4Mn_2Fe(PO_4)_2(P_2O_7)$	solid-state	6.0	2	110 mAh g^{-1} at 0.05 C	84.8% (100th at 0.05 C)	[12]
$Na_3Fe_2(PO_4)(P_2O_7)/RGO$	spray drying	8.26	2	105.5 mAh g^{-1} at 0.2 C	88% (2000th at 10 C)	[13]
$Na_3FeMn(PO_4)(P_2O_7)$	spray drying	5.54	4.5	108 mAh g^{-1} at 0.1 C 79 mAh g^{-1} at 1 C	94.2% (100th at 0.5 C)	[14]
$Na_4Fe_{2.9}Mn_{0.1}(PO_4)_2(P_2O_7)$	solid-state	6.64	2.2-3.5	119.6 mAh g^{-1} at 0.1 C	84.8% (3000th at 10 C)	[4]
$Na_4Fe_{2.85}Mn_{0.15}(PO_4)_2(P_2O_7)$	solid-state	9.48	2.5	111.6 mAh g^{-1} at 0.1 C	88.1% (1000th at 50 C)	[15]

$Na_3Fe_2(PO_4)(P_2O_7)$	sol-gel	14.42	1.5	99.8 mAh g^{-1} at 0.1 C	93.30% (100^{th} at 1 C)	16
$Na_3Fe_{1.9}Ni_{0.1}(PO_4)(P_2O_7)$		16.41		100.7 mAh g^{-1} at 0.1 C	94.12% (100^{th} at 1 C)	
$Na_3Fe_2(PO_4)(P_2O_7)$	sol-gel	7.69	1.2-1.7	93.9 mAh g^{-1} at 0.1 C	70.9% (4000^{th} at 20 C)	17
$Na_3Fe_{1.8}Cr_{0.2}(PO_4)(P_2O_7)$		8.09		113.6 mAh g^{-1} at 0.1 C	92.1% (4000^{th} at 20 C)	
Holey graphene modified NFPP	solid-state	5.97	2.7	118 mAh g^{-1} at 0.2 C	87.4% (200^{th} at 1 C)	3
NFPP-Mg5%	sol-gel	15.0	1.5	104 mAh g^{-1} at 0.05 A g^{-1}	90.4% (5000^{th} at 5 A g^{-1})	6
$Na_3Fe_2(PO_4)(P_2O_7)$/C @RGO	spray drying	-	3-4	110.2 mAh g^{-1} at 0.1 C	89.7% (6400^{th} at 20 C)	18
$Na_4Fe_3(PO_4)_2(P_2O_7)$	sol-gel	6.9	2	110.6 mAh g^{-1} at 0.05 C	92.8% (1000^{th} at 2 C)	19
$Na_4Fe_{2.85}(NiCoMnCuMg)_{0.03}(PO_4)_2P_2O_7$	solid-state	7.28	1.5-2	122 mAh g^{-1} at 0.1 C	82.3% (1500^{th} at 10C)	20
$Na_{3.94}Fe_{2.94}V_{0.06}(PO_4)_2(P_2O_7)$	spray-drying	7.43	1.5	123.4 mAh g^{-1} at 0.1 C	81.65% ($10,000^{th}$ at 20C)	21
$Na_4Fe_3(PO_4)_2(P_2O_7)$	solid-state	2.1	4.3	94.1 mAh g^{-1} at 0.1 C	90.69 (5000^{th} 10C)	22
$Na_4Fe_{2.98}Ti_{0.01}(PO_4)_2(P_2O_7)$		1.8		112.2 mAh g^{-1} at 0.1 C	95.88% (5000^{th} 10C)	

References

1. X. Wu, G. Zhong and Y. Yang, *Journal of Power Sources*, 2016, **327**, 666-674.
2. H. Kim, I. Park, S. Lee, H. Kim, K.-Y. Park, Y.-U. Park, H. Kim, J. Kim, H.-D. Lim, W.-S. Yoon and K. Kang, *Chemistry of Materials*, 2013, **25**, 3614-3622.
3. X. Li, Y. Meng and D. Xiao, *Chemistry – A European Journal*, 2023, **29**, e202203381.
4. Q. Tao, H. Ding, X. Tang, K. Zhang, J. Teng, H. Zhao and J. Li, *Energy & Fuels*, 2023, **37**, 6230-6239.
5. J. Gao, H. Chen, Y. Mei, L. Ni, H. Wang, J. Huang, N. Hong, B. Song, Y. Tian and W. Deng, *Nano Energy*, 2023, **115**, 108747.
6. F. Xiong, J. Li, C. Zuo, X. Zhang, S. Tan, Y. Jiang, Q. An, P. K. Chu and L. Mai, *Advanced Functional Materials*, 2023, **33**, 2211257.
7. J. Zhang, L. Tang, Y. Zhang, X. Li, Q. Xu, H. Liu and Z.-F. Ma, *Journal of Power Sources*, 2021, **498**, 229907.
8. P. Barpanda, T. Ye, S.-i. Nishimura, S.-C. Chung, Y. Yamada, M. Okubo, H. Zhou and A. Yamada, *Electrochemistry Communications*, 2012, **24**, 116-119.
9. Z. Liu, Y. Cao, H. Zhang, J. Xu, N. Wang, D. Zhao, X. Li, Y. Liu and J. Zhang, *ACS Sustainable Chemistry & Engineering*, 2024, **12**, 1132-1141.
10. T. Yuan, Y. Wang, J. Zhang, X. Pu, X. Ai, Z. Chen, H. Yang and Y. Cao, *Nano Energy*, 2019, **56**, 160-168.
11. Y. Cao, X. Xia, Y. Liu, N. Wang, J. Zhang, D. Zhao and Y. Xia, *Journal of Power Sources*, 2020, **461**, 228130.
12. H. Kim, G. Yoon, I. Park, J. Hong, K.-Y. Park, J. Kim, K.-S. Lee, N.-E. Sung, S. Lee and K. Kang, *Chemistry of Materials*, 2016, **28**, 7241-7249.
13. H. Wang, Z. Pan, H. Zhang, C. Dong, Y. Ding, Y. Cao and Z. Chen, *Small Methods*, 2021, **5**, 2100372.
14. N. Wang, J. Ma, Z. Liu, J. Xu, D. Zhao, N. Wang, C. Yang, Y. Cao, J. Lu and J. Zhang, *Chemical Engineering Journal*, 2022, **433**, 133798.
15. J. Gao, H. Chen, Y. Mei, L. Ni, H. Wang, J. Huang, N. Hong, B. Song, Y. Tian, W. Deng, G. Zou, H. Hou and X. Ji, *Nano Energy*, 2023, **115**, 108747.
16. X. Wang, H. Li, W. Zhang, X. Ge, L. He, L. Zhang, S. Li, N. Wen, J. Guo, Y. Lai, S. Li and Z. Zhang, *Journal of Materials Chemistry A*, 2023, **11**, 6978-6985.
17. B. Zhang, G. Chen, Y. Yang, M. Liu, X. Li, H. Liu and Z.-F. Ma, *ACS Sustainable Chemistry & Engineering*, 2023, **11**, 10083-10094.
18. Y. Cao, C. Yang, Y. Liu, X. Xia, D. Zhao, Y. Cao, H. Yang, J. Zhang, J. Lu and Y. Xia, *ACS Energy Letters*, 2020, **5**, 3788-3796.
19. J. Gao, Y. Mei, L. Ni, H. Wang, B. Song, W. Deng, G. Zou, H. Hou and X. Ji, *Inorganic Chemistry*, 2023, **62**, 9099-9110.
20. X. Ge, H. Li, J. Li, C. Guan, X. Wang, L. He, S. Li, Y. Lai and Z. Zhang, *Small*, 2023, 2302609.
21. H. Zhang, Y. Cao, Z. Liu, X. Cheng, X.-L. Li, J. Xu, N. Wang, H. Yang, Y. Liu and J. Zhang, *ACS Sustainable Chemistry & Engineering*, 2024, **12**, 5310-5318.
22. Y. Han, X. Wang, W. Yan, A. L. Buzlukov, P. Hu, L. Zhang, J. Yu and T. Liu, *ACS Applied Materials & Interfaces*, 2024, DOI: 10.1021/acsami.4c05943.